Venus Nightside Ionosphere

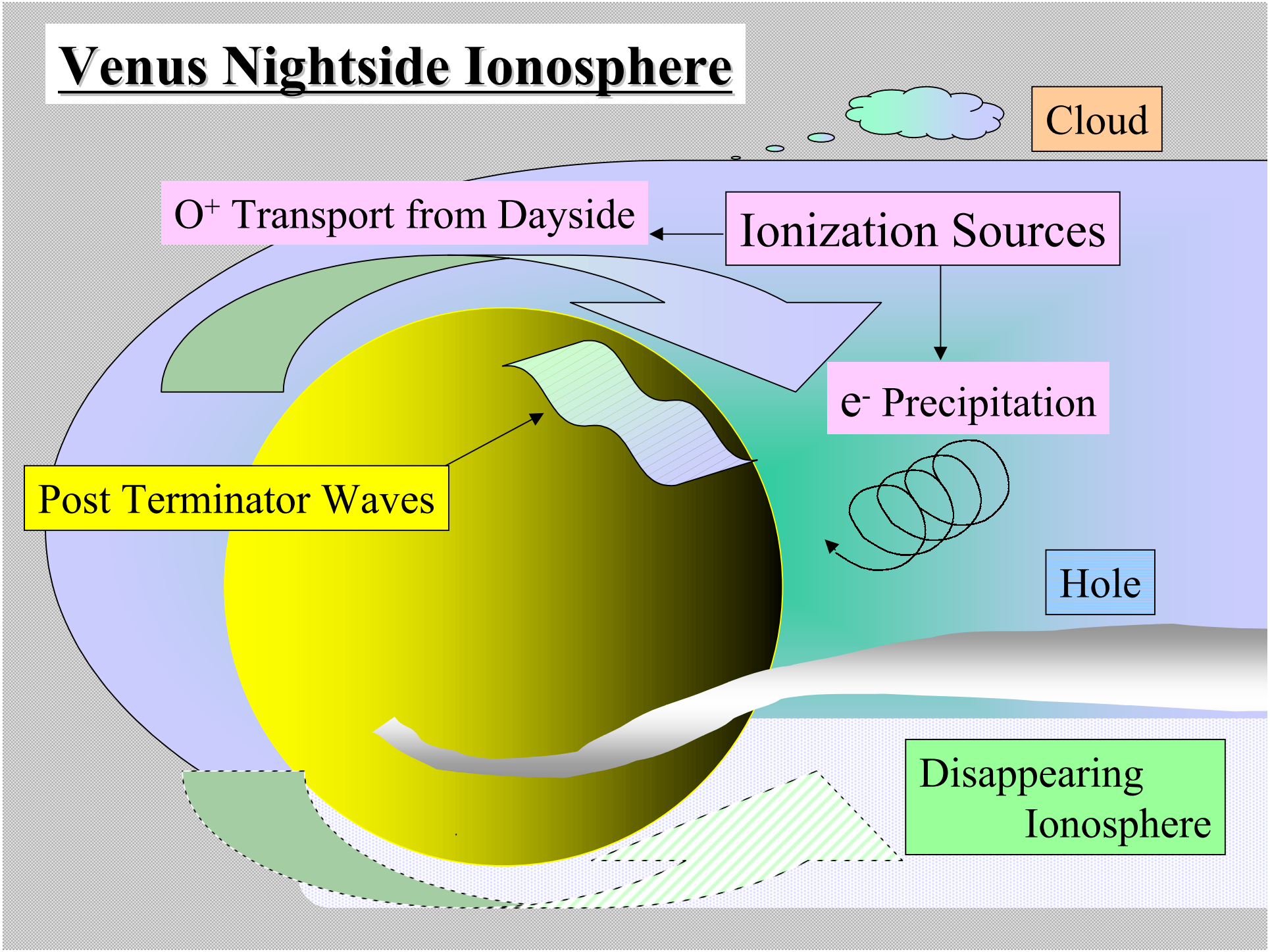

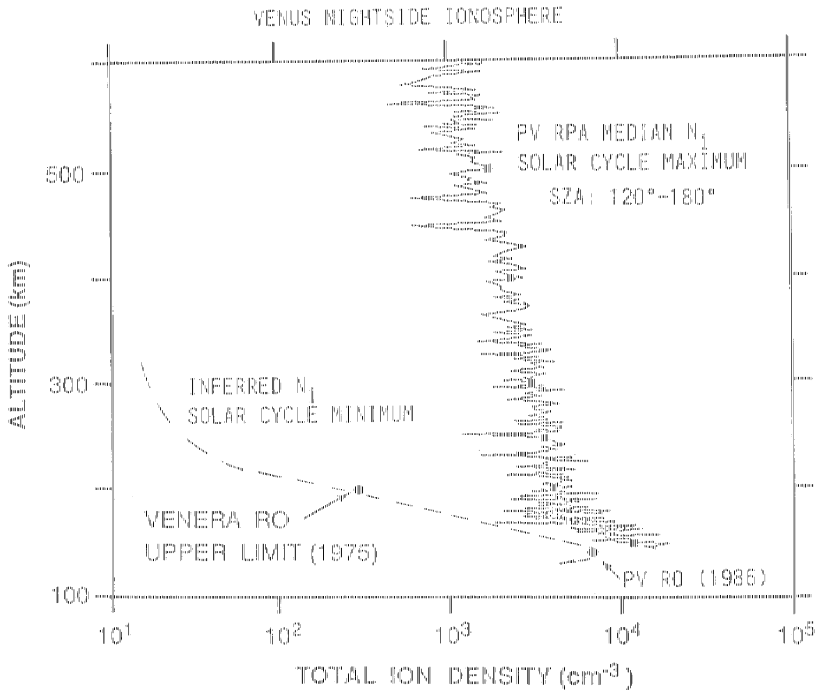

Fig. 37. Comparison of the solar maximum median nightside ion density altitude profile measured by the PVO ORPA, the solar minimum average peak electron density measured by the PVO radio occultation experiment [A. J. Kliore, private communication, 1987], and upper limit of the electron density at and above 200 km altitude at solar minimum inferred from Venera 9 and 10 radio occultation profiles [Savich et al., 1982].

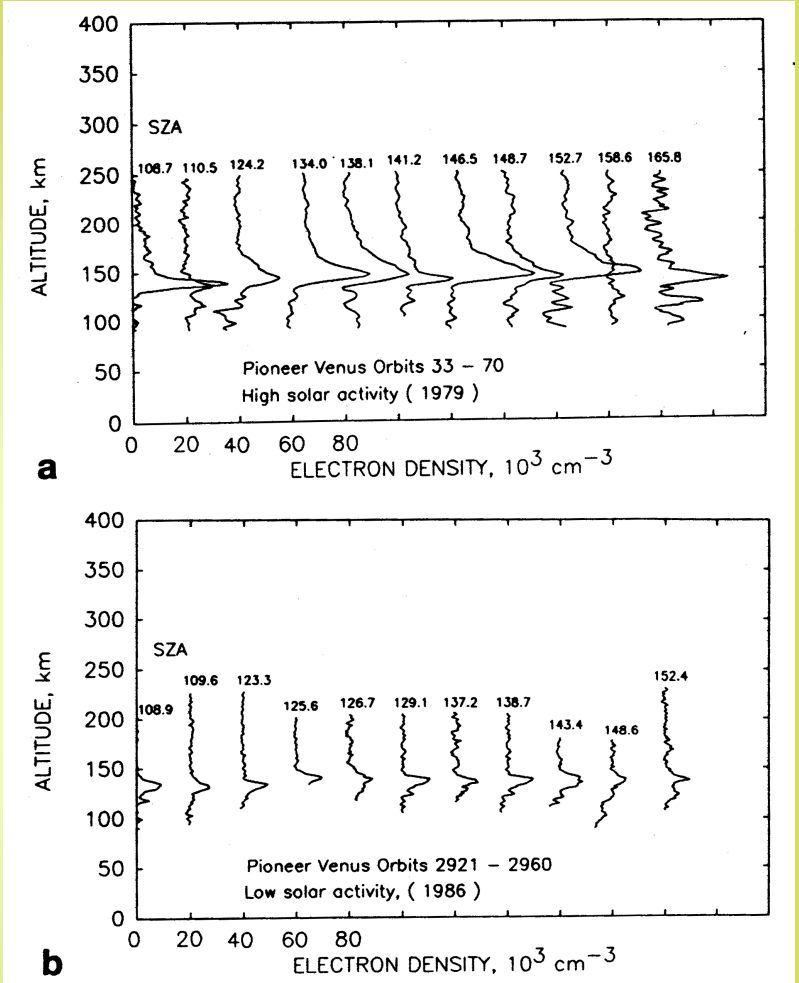

Fig. 8. Vertical electron density profiles in the deep nightside ionosphere of Venus as observed with Pioneer Venus. (a) high solar activity (1979); (b) low solar activity (1986).

夜側の電子密度プロファイル

PVOによる観測例（太陽活動度極大期はORPA、極小期は電波掩蔽観測による）。[Knudsen, 1992]
太陽活動度極大期に比べて、極小期は150kmより高高度では急激に電子密度が減少。

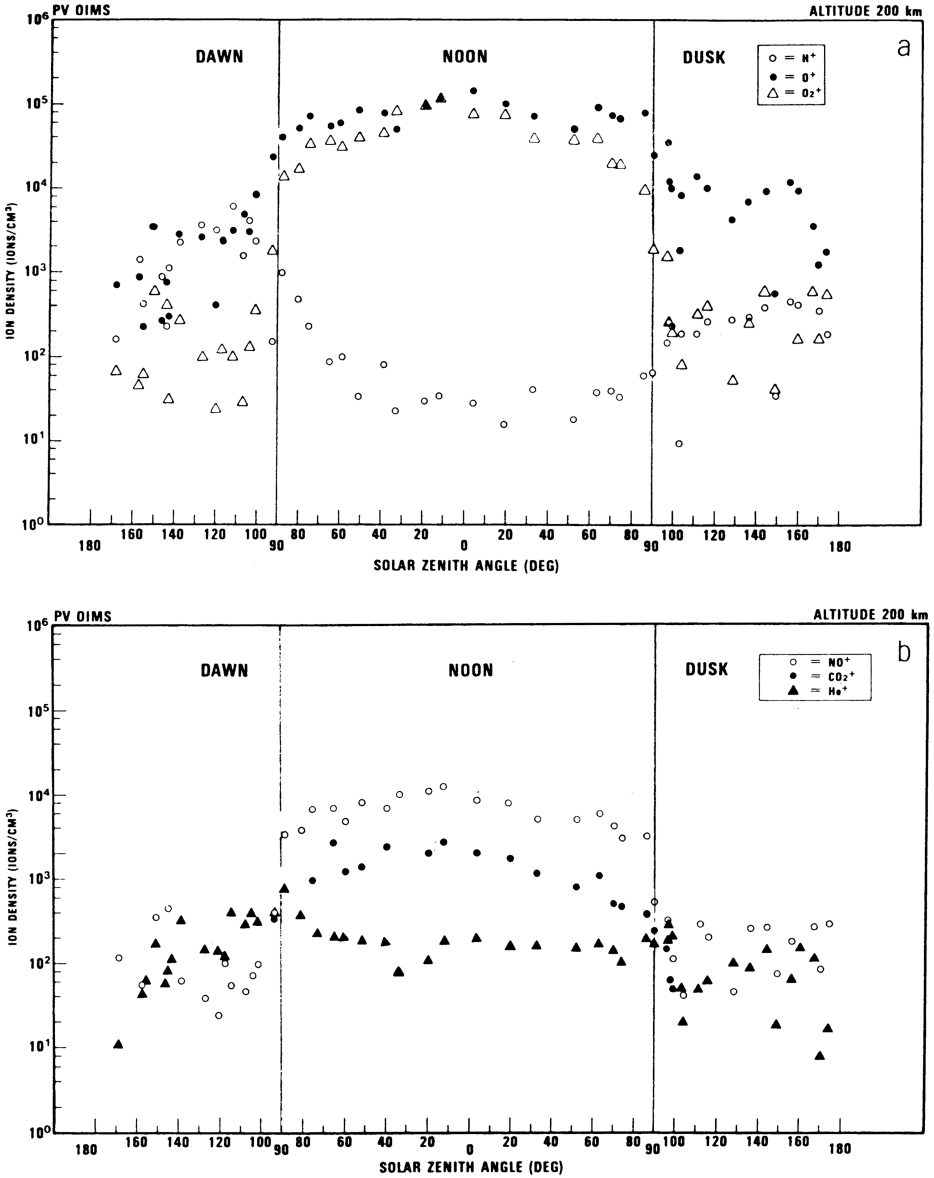

Fig. 18. (a,b) Variation of several ion species with SZA for a fixed altitude of 200 km as measured by the OIMS at solar maximum. The measurements were taken from the outbound leg of orbits at a latitude of 8° N and represent, for the most part, quiet conditions (from [Taylor et al., 1980a]).

イオン密度のSZA依存 [Taylor et al., 1980]

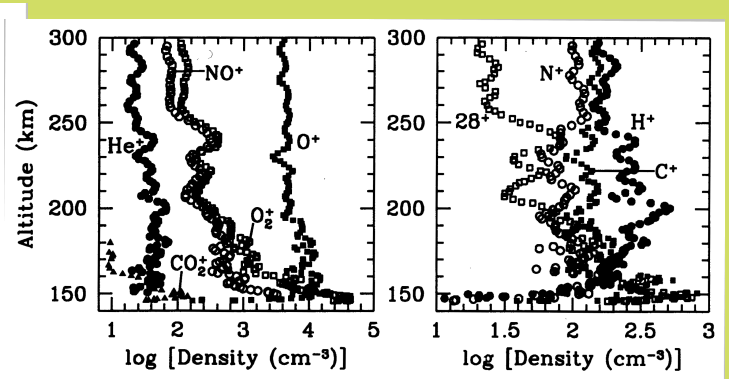

Figure 8. Smoothed OIMS ion density profiles from orbit 506. At periapsis, the SZA was 150.9° and the local time was 22.2 hr.

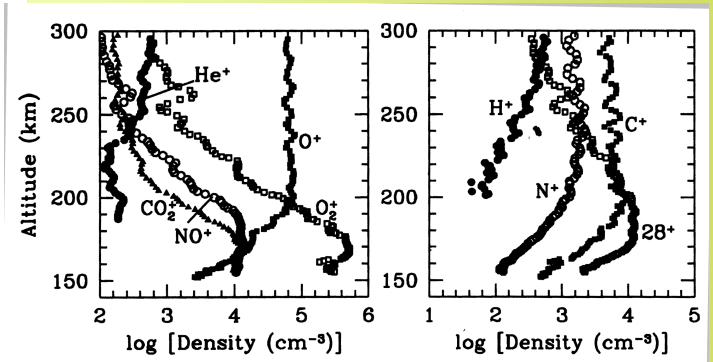

Figure 1. Smoothed ion density profiles measured by the OIMS on orbit 200. The solar zenith angle at periapsis was 25.7°, and the local time was about 13.4 hr. 28^+ denotes $CO^+ + N_2^+$.

夜側のイオンの測定

（PVO OIMSによる観測例）[Fox,1997]

低高度ではO_2^+、高高度ではO^+ がdominant,

昼側（下）と主成分は同じ。

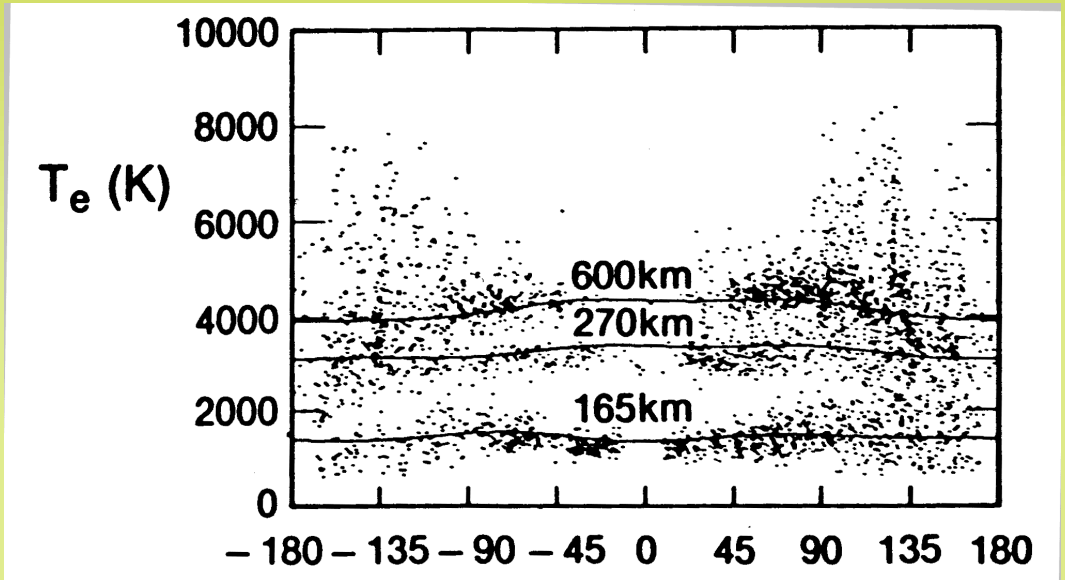

Fig. 23. Total electron temperature measured by the OETP within three altitude intervals, 160 -170, 260 - 280, and 550 - 650 km as a function of SZA. The solid lines are empirical model values at the indicated altitudes derived from median values of the individual measurements, the latter indicated by the dots. The data base consists of measurements within the ionosphere from Dec 1978 to Dec 1982, the period of solar maximum (adapted from [Theis et al., 1984]).

電子温度、イオン温度のプロファイル（次ページ2枚含む）

- 夜側の電子温度の変動が大きい。[Theis et al., 1984; Miller et al., 1980]
  Hole, Disappearing Ionosphereによる電子密度変動が原因？
- 夜側のイオン温度が高い。[Miller et al., 1980]
  中性大気によるlossが少なくなるから。
  また、昼側から夜側へのイオン流の運動エネルギーが熱に変換。

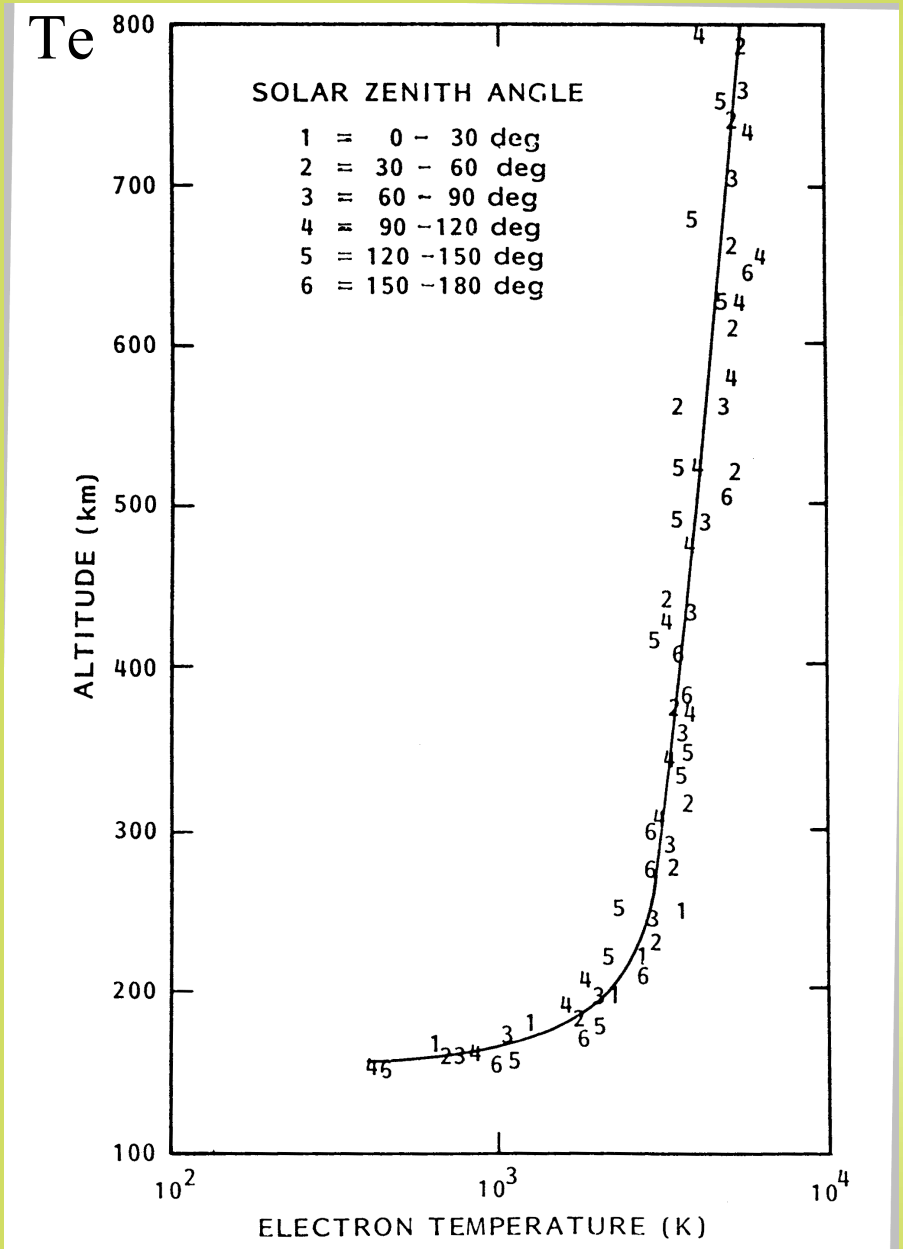

Fig. 24. Vertical profiles of median electron temperatures as a function of SZA at solar maximum (from [Miller et al., 1980]).

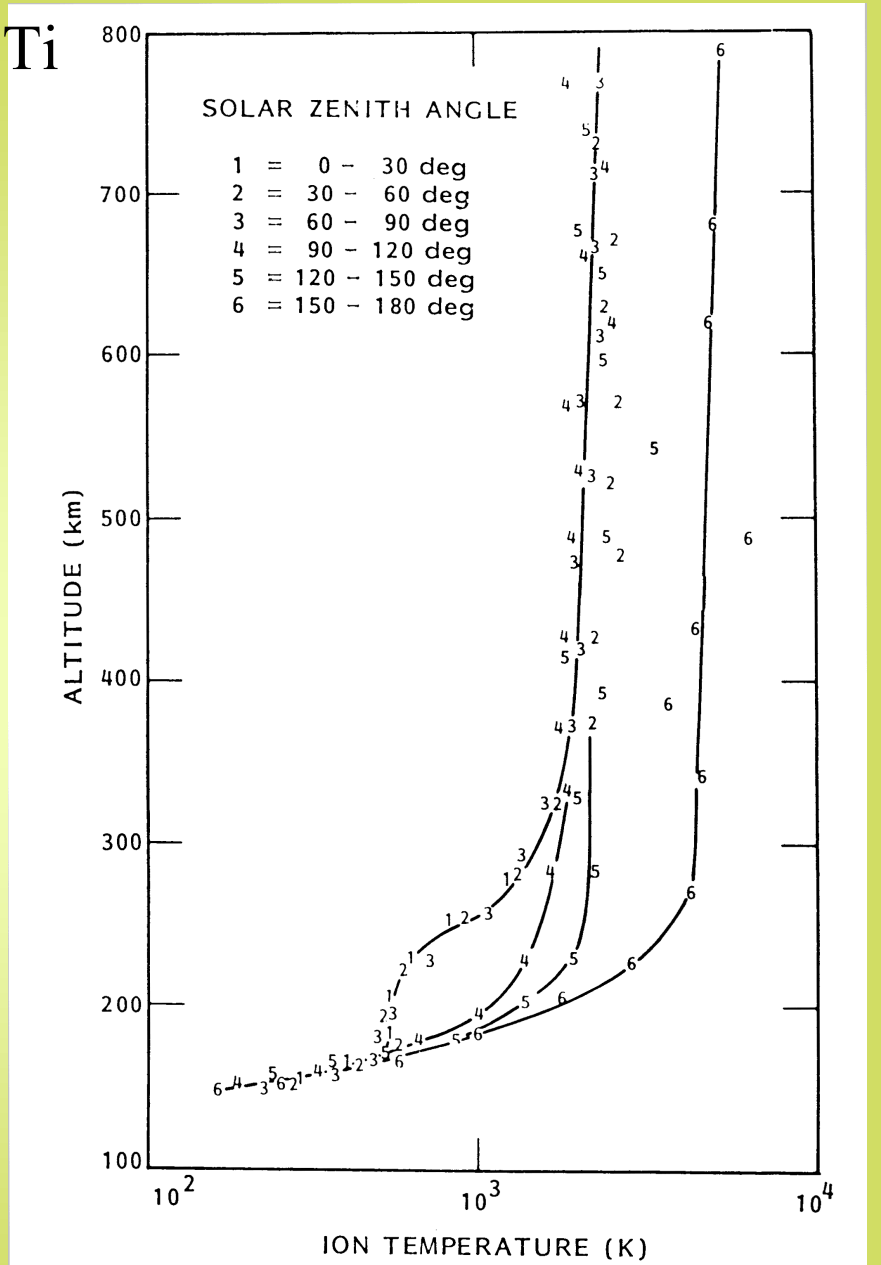

Fig. 25. Vertical profiles of median ion temperatures as a function of SZA at solar maximum (from [Miller et al., 1980]).

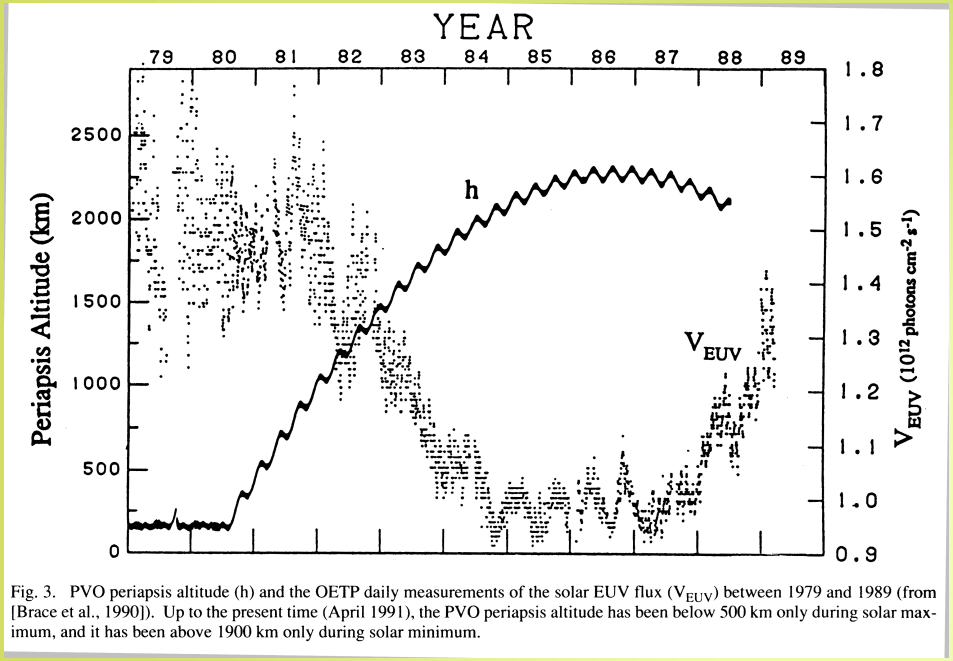

Fig. 3. PVO periapsis altitude (h) and the OETP daily measurements of the solar EUV flux (V_{EUV}) between 1979 and 1989 (from [Brace et al., 1990]). Up to the present time (April 1991), the PVO periapsis altitude has been below 500 km only during solar maximum, and it has been above 1900 km only during solar minimum.

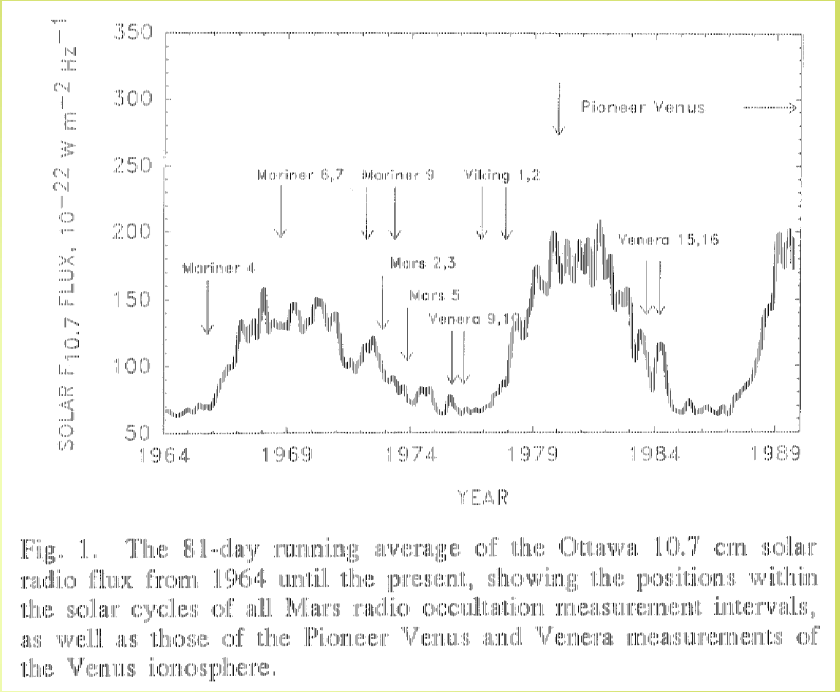

Fig. 1. The 81-day running average of the Ottawa 10.7 cm solar radio flux from 1964 until the present, showing the positions within the solar cycles of all Mars radio occultation measurement intervals, as well as those of the Pioneer Venus and Venera measurements of the Venus ionosphere.

PVO近金点高度と太陽活動度

PVOが低高度の直接観測ができたのは、太陽活動度が高い時のみ。[Knudsen, 1992]

金星、火星探査機の観測時期と太陽活動度

金星は極大期、極小期ともに観測がある。
火星の夜側電離圏を検出したMars 4, 5及びVikingは、ともに太陽活動度が低い時だった。[Kliore, 1992]

Nightside Ionization Sources

太陽活動度が
極大期～昼側→夜側への酸素原子イオンfluxが主
極小期～夜側大気への低エネルギー電子の降込が主

太陽活動度極大期には、電離源としては、昼夜輸送が電子降り込みの３倍くらい利いている[Knudsen, 1992]

問題点
- PVOの低エネルギー電子の観測はomnidirectional、どのくらいの量が実際には降り込んでいるのか？
- 低エネルギー電子の発生源もわかっていない

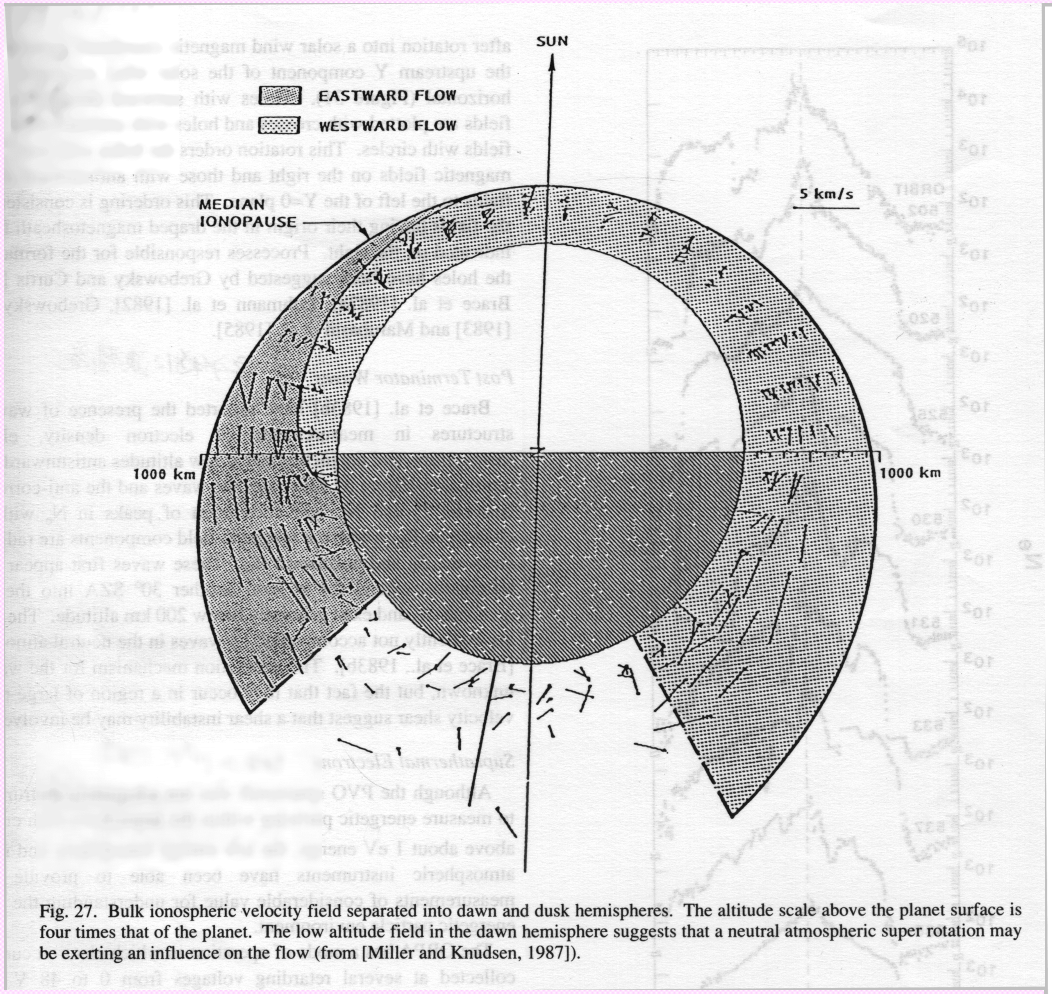

Fig. 27. Bulk ionospheric velocity field separated into dawn and dusk hemispheres. The altitude scale above the planet surface is four times that of the planet. The low altitude field in the dawn hemisphere suggests that a neutral atmospheric super rotation may be exerting an influence on the flow (from [Miller and Knudsen, 1987]).

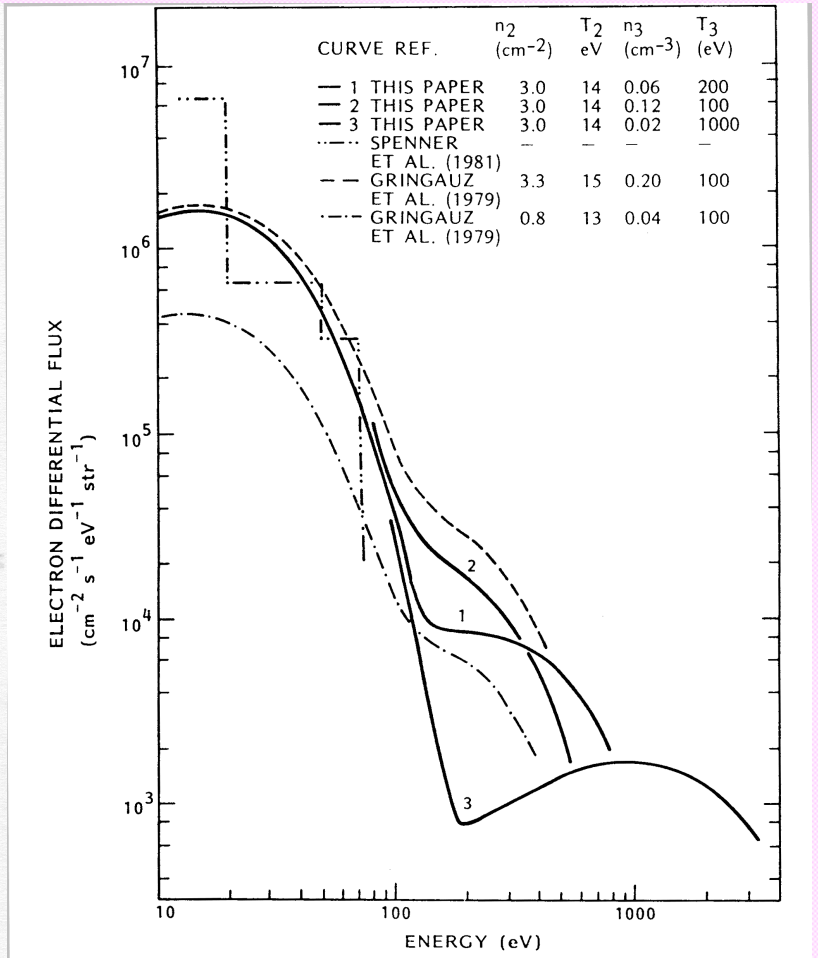

Fig. 34. Median suprathermal electron energy spectra measured in the Venus umbra at solar maximum in the altitude interval 1000-2000 km by the PVO ORPA and at solar minimum by the Venera 9 and 10 hemispherical retarding potential analyzer (adapted from [Knudsen and Miller, 1985]).

夜側への酸素原子イオンの輸送

太陽活動度が極大期に、昼側→夜側への酸素原子イオンのfluxを観測。
[Knudsen et al., 1982]

夜側での低エネルギー電子の観測

RPAにより高高度で、数十eVの電子のfluxを観測。
[Knudsen and Miller, 1985]

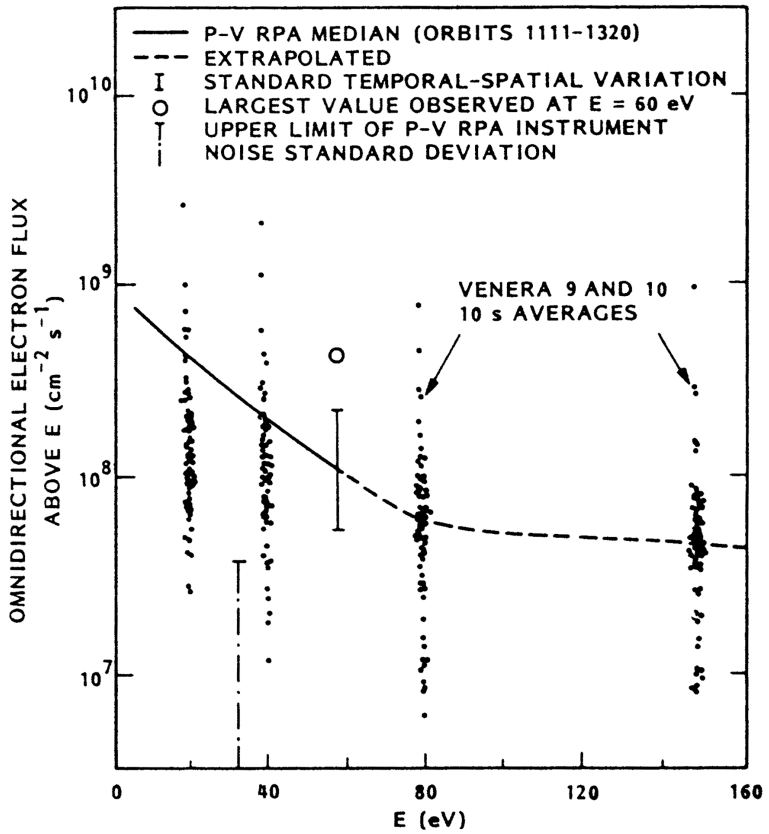

Fig. 7. Comparison of the median P-V RPA omnidirectional electron flux and variation derived in this study with measurements made on Venera 9 and 10 (K. I. Gringauz et al., unpublished manuscript, 1982). The extrapolated portion of the P-V curve is computed from the measured median value of n_3 at $E = 60$ eV and an assumed T_3 of 200 eV (see text).

太陽活動度と低エネルギー電子のflux

観測では電子のfluxは太陽活動度によらず存在。
40eV以下の電子だと、極大期は極小期の2倍程度。
[Knudsen and Miller, 1985]

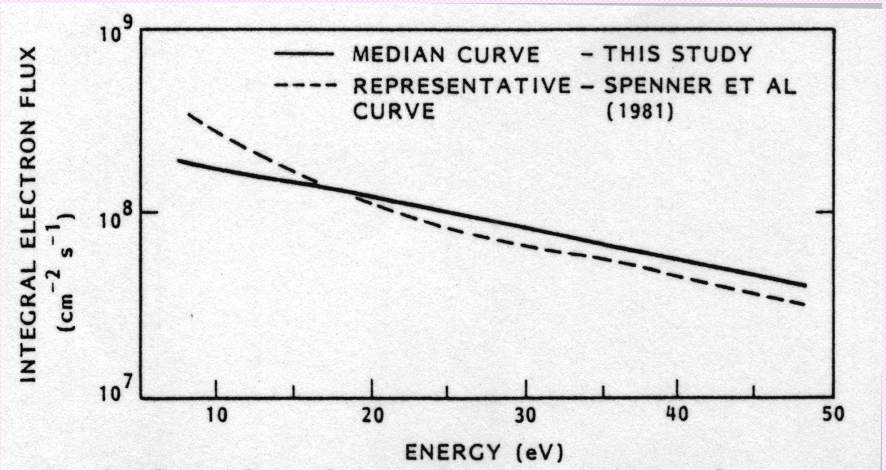

Fig. 6. Comparison of the median integral electron flux energy distribution curve from this study with the representative curve derived in a previous study at lower altitude by *Spenner et al.* [1981].

高度による低エネルギー電子のfluxの違い

点線が低高度(200-800km)、実線が高高度(1000km)。
[Knudsen and Miller, 1985]

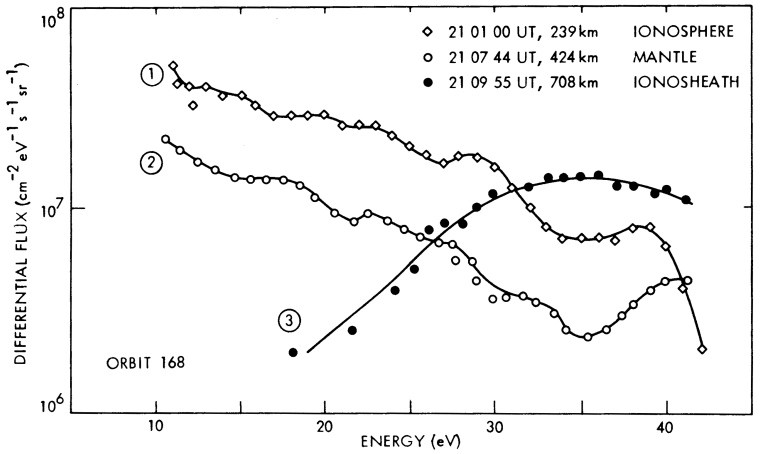

Fig. 13. Change in differential electron flux as the PVO spacecraft passed from the ionosphere into the ionosheath (magnetosheath) at solar maximum (from [Spenner et al., 1980]). The spectrum changed from one characteristic of ionospheric photoelectrons to one characteristic of the ionosheath electrons.

電子のエネルギースペクトルの違い

Ionosphere, Mantle, Ionosheathでの電子のスペクトル。[Knudsen and Miller, 1985]

Hole

電子密度が大きく減少

Hole中の
イオン速度・温度の
データが不足

Hole中の磁場と電子・イオン温度

磁場は強化されラジアル方向を向いている。
電子温度は高温成分（非Maxwellian）と低温成分(Maxwellian)とが観測されている。
イオン温度は減少、しかし観測数は少ない。
[Luhmann et al., 1982]

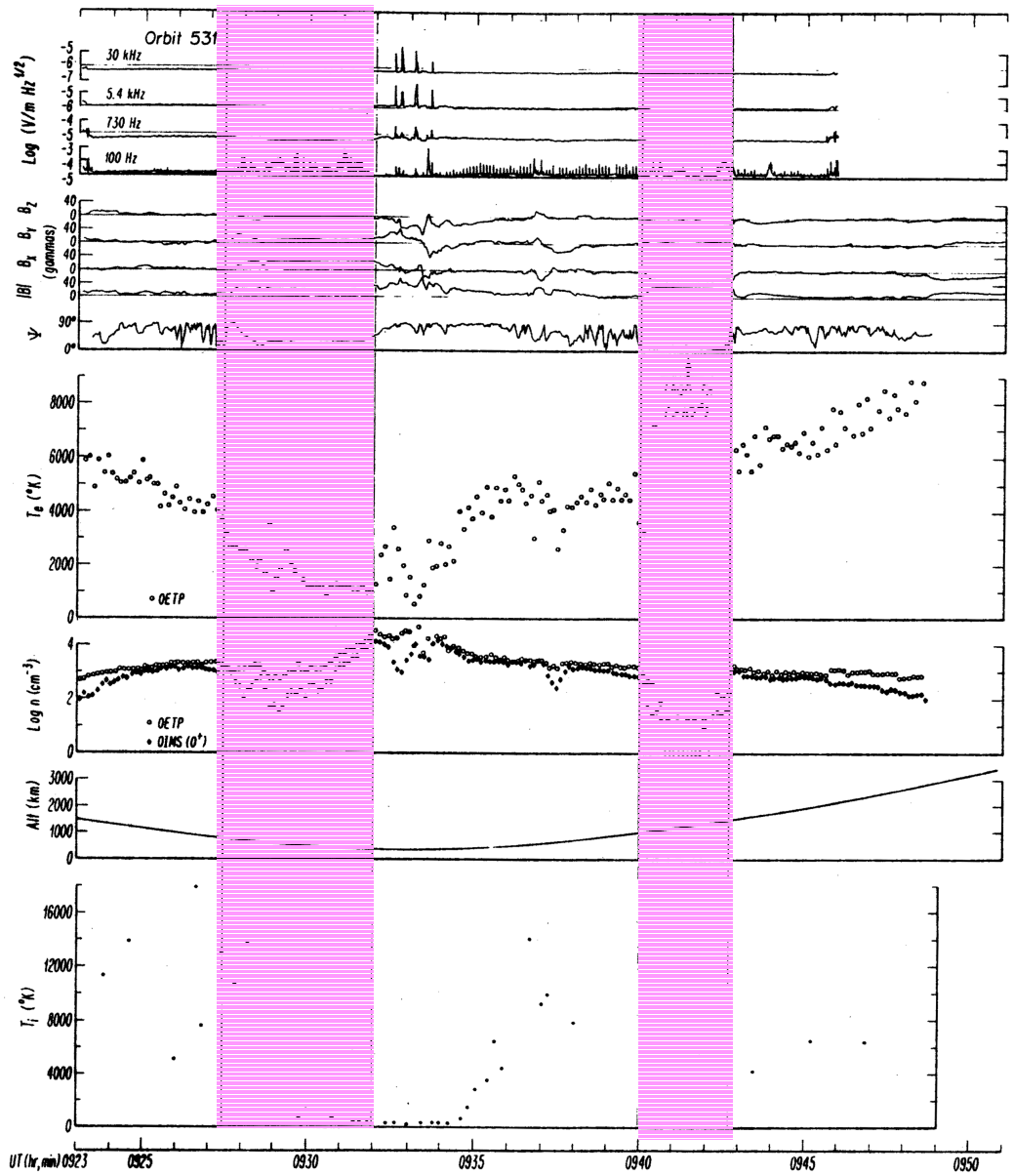

Fig. 2. Same as Figure 1 but for orbit 531, with the addition of ion temperature (T_i) measurements from the retarding potential analyzer (bottom). Note the similarity of this orbit to orbit 530 (Figure 1), which occurred 24 hours earlier.

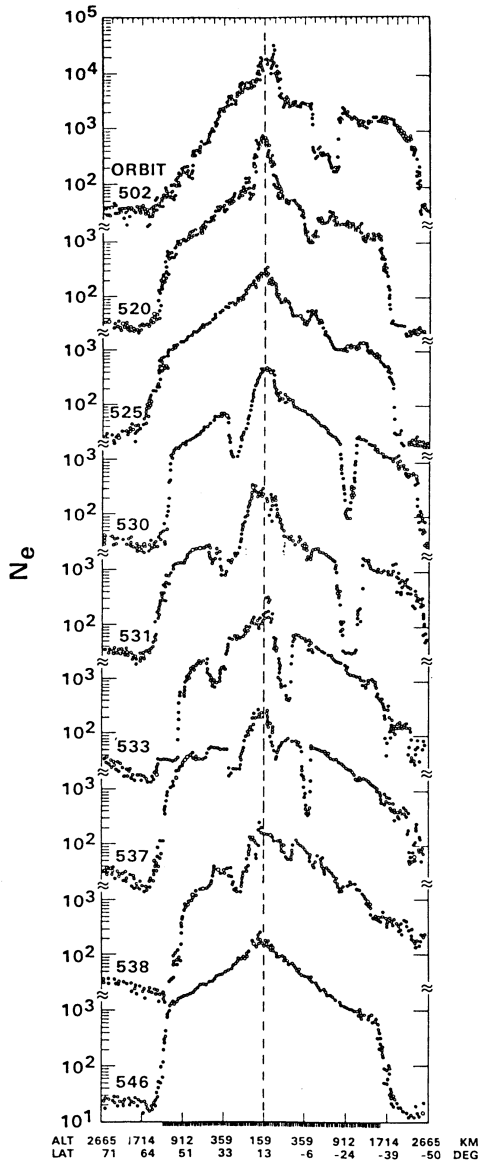

Fig. 29. Ionospheric holes present in several orbits that otherwise exhibit a fully established nightside ionosphere (from [Brace et al., 1982b]).

Hole中の電子密度

[Brace et al., 1982]

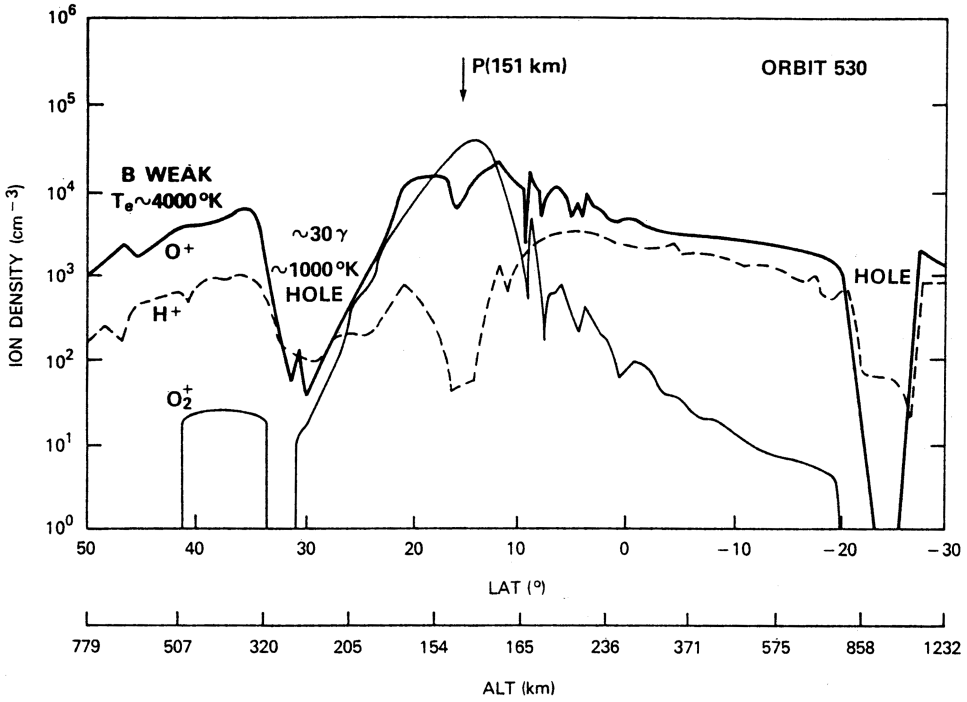

Fig. 1. Pioneer Venus traversal of two holes. The concentrations of O^+, H^+ and O_2^+ (which is minor in concentration except as periapsis P is approached) is plotted as a function of latitude. O^+ is generally the major ion outside the holes while H^+ becomes more dominant within them. The magnetic field on this orbit became intensified within the inbound and outbound detected holes, while the electron temperature cooled [Luhmann et al., 1982].

Hole中のイオン組成

周囲の環境では酸素原子イオンが多いのに対し、Hole中では水素原子イオンが増加。[Luhmann et al., 1982]

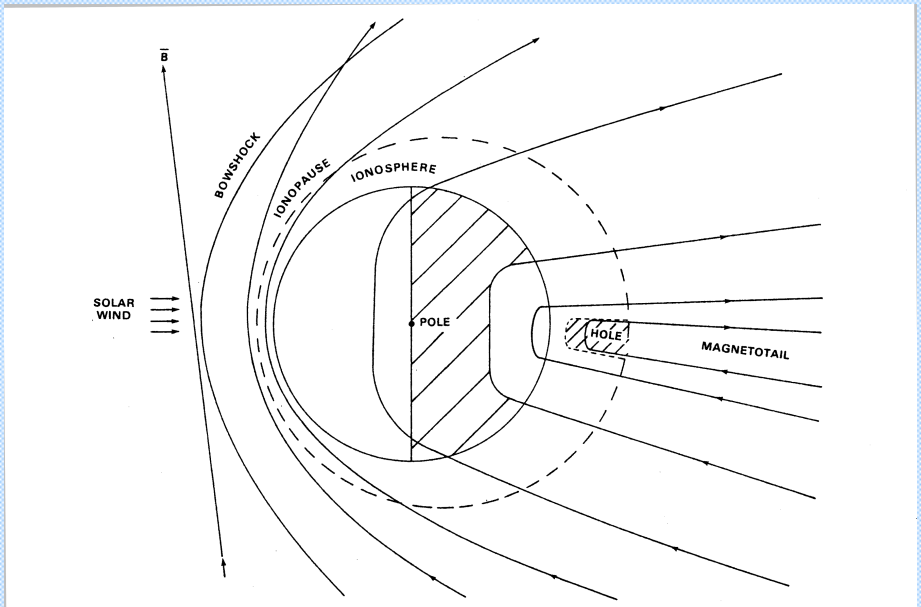

Fig. 11. A conceptual view of the evolution of an interplanetary field line entering the northern dayside ionosphere, convecting over the northern polar cap, and pulling out of the ionosphere to form a hole on the nightside somewhere north of the equator. Those field lines which convect over the southern pole would form a similar hole south of the equator. Thus conjugate north-south pairs of holes would be expected.

IMFのDrapeによるHoleの生成（概念図）

[Brace et al., 1982]

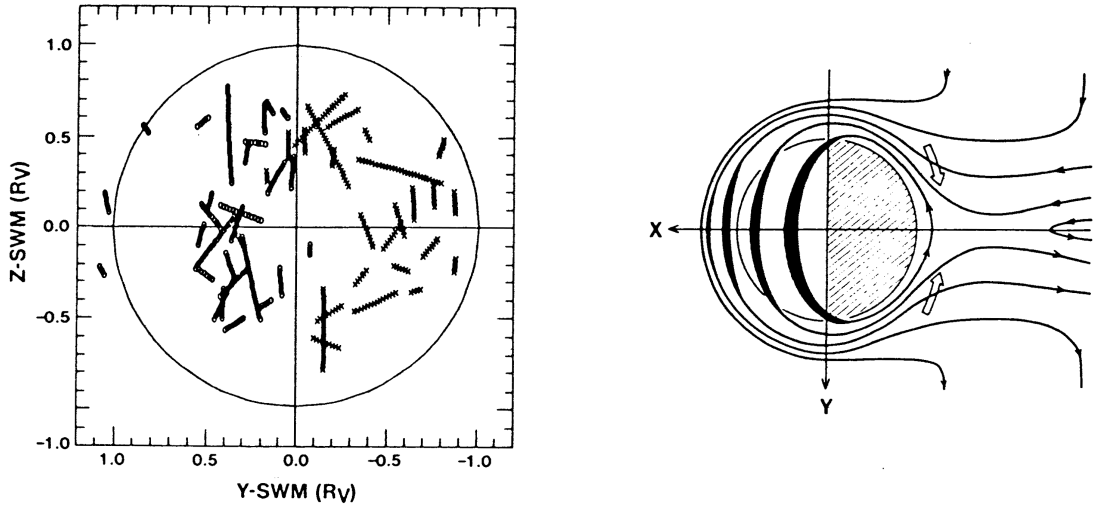

Fig. 31. PVO orbit segments where holes were detected are projected onto the nightside planet after rotation into the Y-Z plane of the solar wind magnetic coordinate system (left). Holes with magnetic field directed sunward are plotted with crosses, and holes with magnetic field directed antisunward, with circles. This organization of the segments is consistent with the hole magnetic fields originating in the draped solar wind magnetic field (right) (adapted from [Marubashi et al., 1985]).

IMFとHole中の磁場極性

Holeの磁場極性は朝側と夕側とで逆転。IMFがDrapeした結果と考えると理解しやすい。[Marubashi et al., 1985]

Disappearing Ionosphere

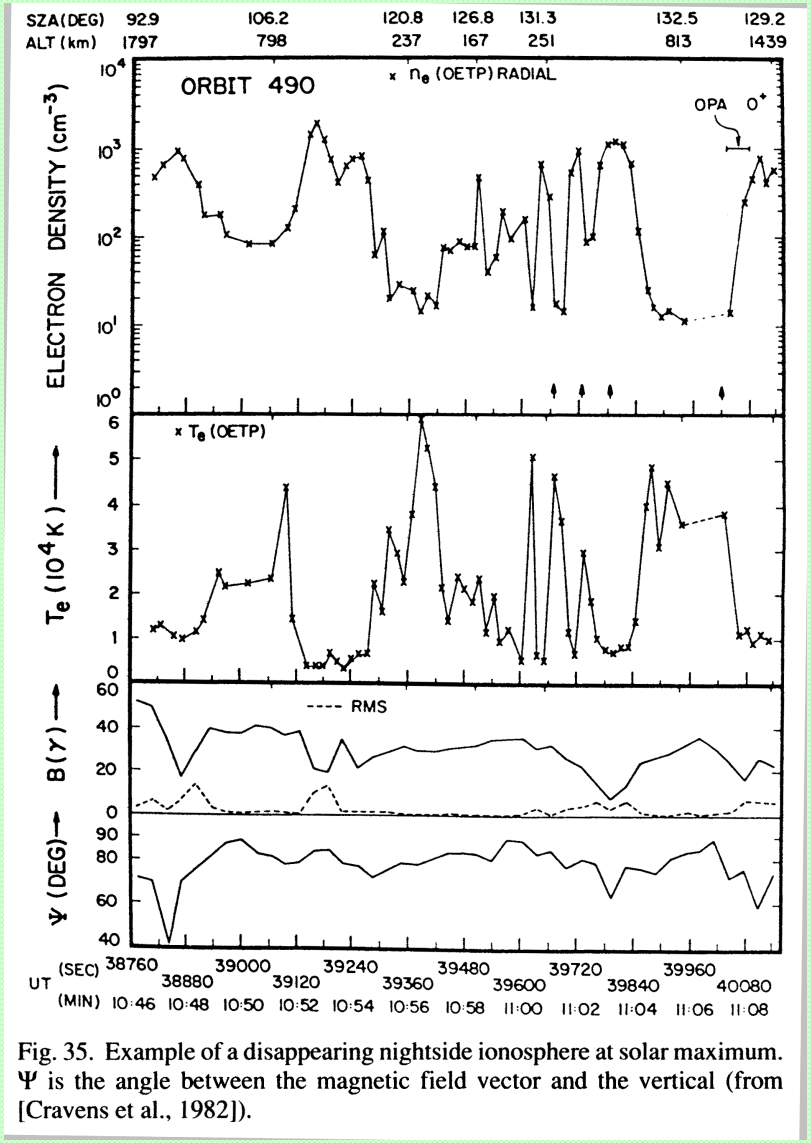

Fig. 35. Example of a disappearing nightside ionosphere at solar maximum. Ψ is the angle between the magnetic field vector and the vertical (from [Cravens et al., 1982]).

Holeと違い、全体的に夜側電離圏の電子密度が小さくなる現象

太陽風の動圧が大きい時に多く観測

Ionopause高度が下がり、昼側からの輸送が減少

しかし、太陽EUVと夜側電子密度は逆相関

Disappearing Ionosphereの電子密度、電子温度と磁場

電子密度は通常は高度140kmで2×10^4[cm^{-3}]程度である。電子温度は密度と逆相関で、密度減少時には大変高温になっている。磁場は、水平方向を向きコヒーレントであり、通常よりも大きい。[Cravens et al., 1982]

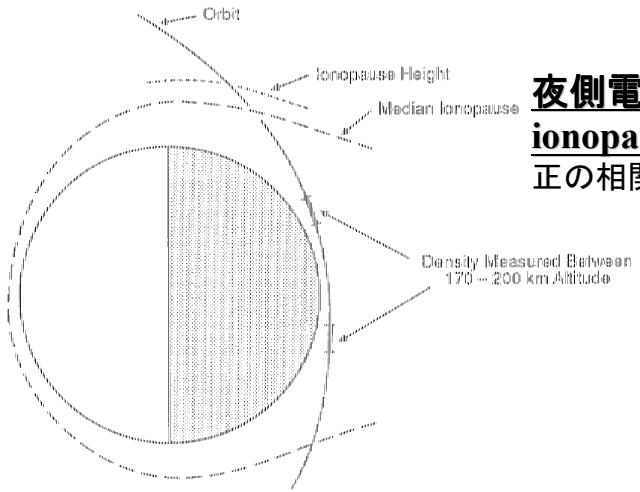

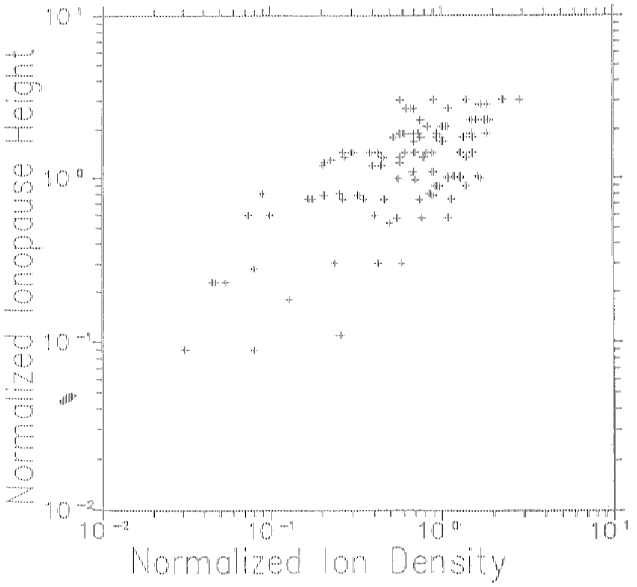

Fig. 36. Correlation of normalized nightside ion density and normalized ionopause height at solar maximum (adapted from [Miller and Knudsen, 1987]. The ion density, measured by the ORPA in the altitude interval 170-200 km, is predominantly O^+ and is normalized by dividing it by the empirical model density of Theis et al. [1984]. The measured ionopause altitude is normalized by dividing it by the median altitude modeled by Knudsen et al. [1982b].

夜側電子密度とterminator付近のionopause高度（左図）

正の相関がある。[Knudsen et al., 1982b]

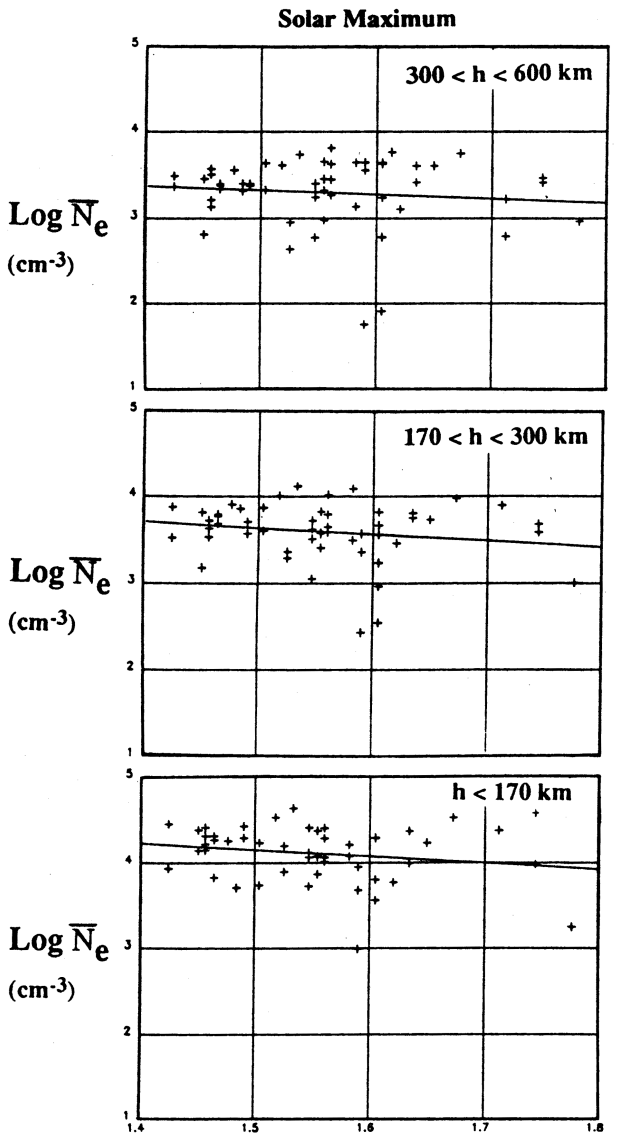

Fig. 8. The orbit to orbit variations of $\bar{N}_e$ in the nightside ionosphere in response to V_{EUV} changes, for three altitude ranges at solar maximum (interval A). $\bar{N}_e$ varies slightly inversely with the EUV flux, a behavior that brings into question the concept that nightward ion flow maintains the nightside ionosphere.

夜側電子密度と太陽EUV flux（右図）

電子密度は、太陽EUVと弱い負の相関。

[Brace et al., 1990]

Post Terminator Waves

Terminatorから夜側に少し入った領域で、密度や電子温度、磁場に波構造が見られる。

メカニズムはわかっていない。
(シアーが原因？)

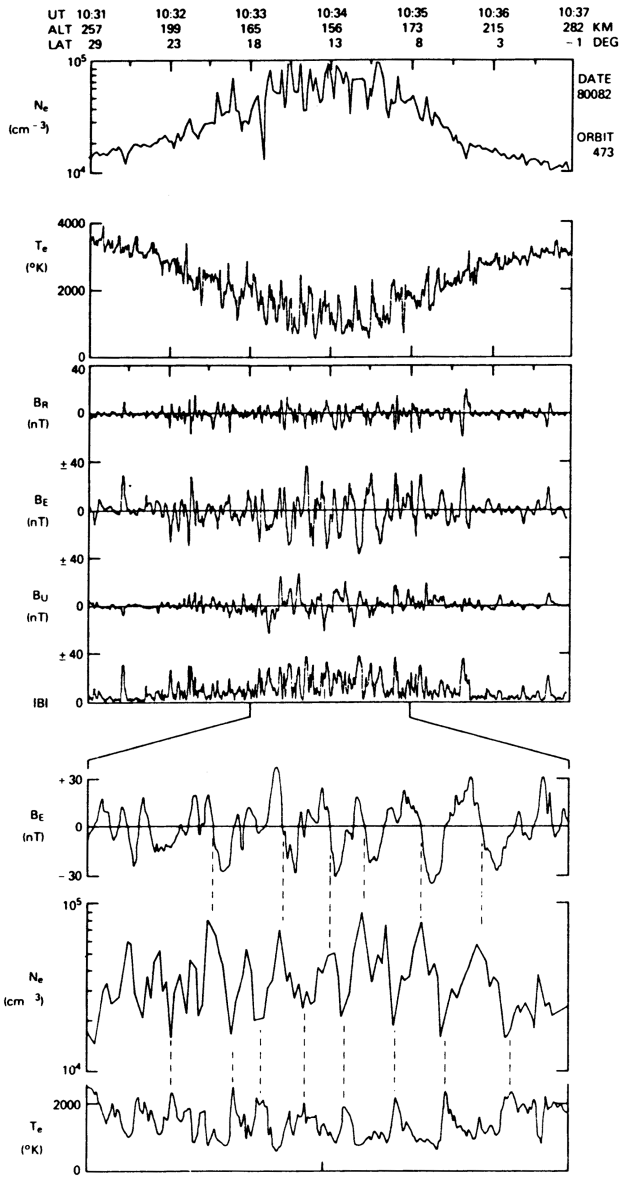

Fig. 32. The ionospheric and magnetic characteristics of post-terminator waves in orbit 473 (SZA=100° at periapsis). The upper five traces show a 6-minute segment of N_e, T_e, B_R, B_E, B_U, and |B|, while the lower panels display and expanded view of N_e, T_e, and B_E which show details of the wave patterns. Well ordered waves develop below about 175 km altitude. The vertical dashed lines draw attention to persistent phase relationships between B_E, N_e, and T_e (from [Brace et al., 1983b]).

電子密度、電子温度、磁場における波構造
[Brace et al., 1983]

Cloud

電離圏からプラズマがちぎれて飛んで行くように見える現象

太陽風との相互作用で発生？

特徴（以下の全てが現われるとは限らない）

- 磁場のX成分の極性が反転
- 磁場の強度が弱くなる
- 電場スペクトルが強くなる

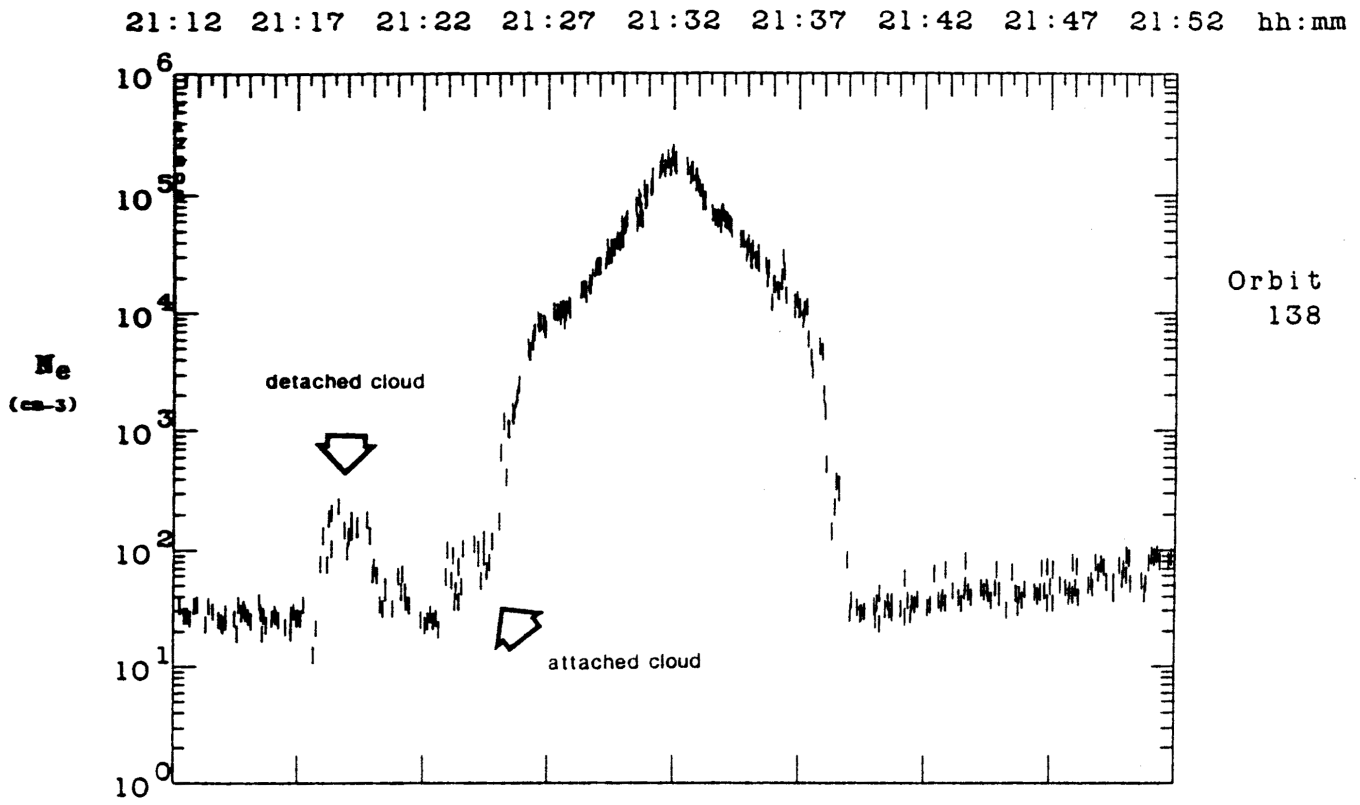

Fig. 1. Sample time series of PVO Langmuir probe data showing "attached" and "detached" cloud signatures.

Cloudの観測

Ionopauseに付着しているように見えるAttached Cloudと、離れているように見えるDetached Cloudが観測されている。
[Ong et al., 1991]

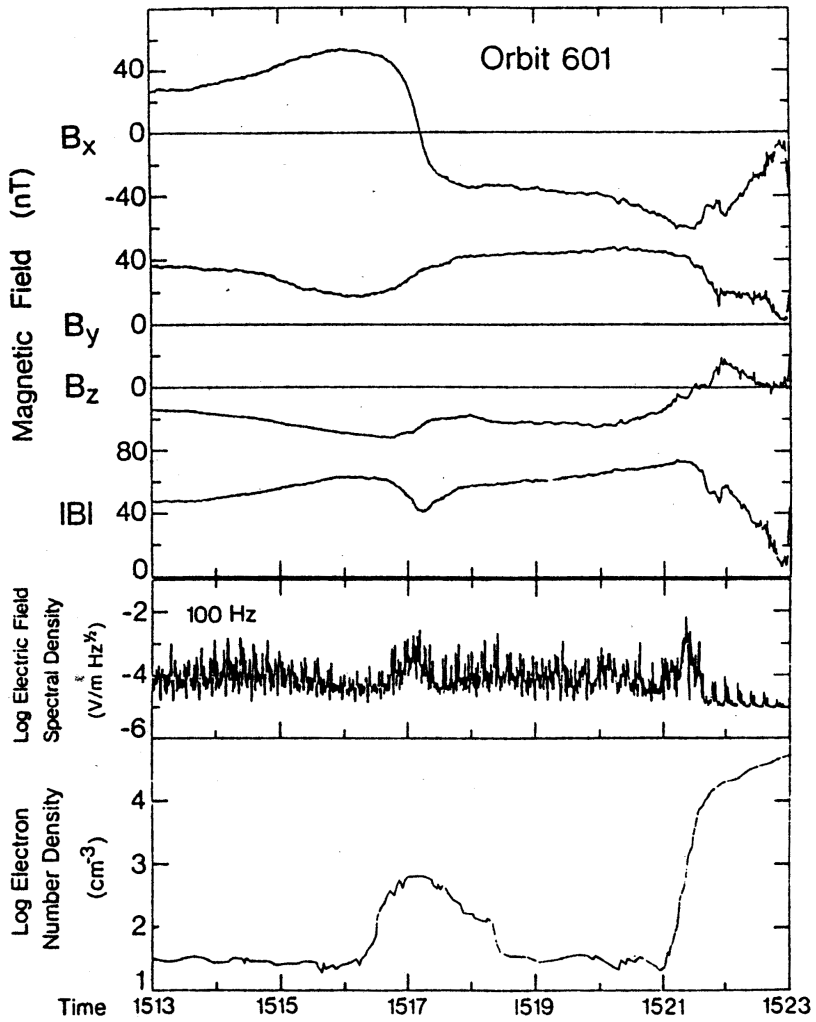

Fig. 2. Example of a classic "detached" cloud (orbit 601) showing electron density, magnetic field, and plasma wave signatures [From Russell et al., 1982].

Cloud中の磁場と電場スペクトル

磁場極性が逆転し、プラズマ波動が観測されている。[Russell et al., 1982]

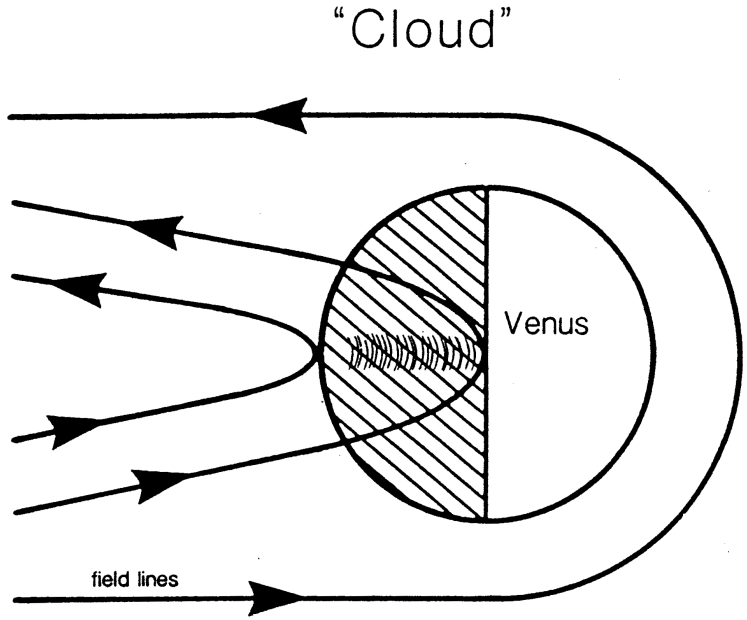

Fig. 3. Schematic illustration of a mechanism for cloud formation. The J x B force associated with the draped magnetic field provides a "magnetic slingshot" which pulls plasma away from the ionosphere proper.

Cloudの生成の概念図

IMFがdrapeし、Ionopauseからプラズマを剥ぎ取って行く。
（磁力線のSlingshot効果）[Ong et al., 1991]

Martian Nightside Ionosphere

Viking, Mars 4, 5
電波掩蔽観測において夜側電離圏を検出
peak密度～5×10^3[cm^{-3}], 観測数少ない
下層電離圏のイオン組成直接測定はない

火星夜側電離圏の生成メカニズム

金星からの類推として
- 昼側からのプラズマの輸送
- 夜側大気への低エネルギー電子の降込

上記の観測はあるか？

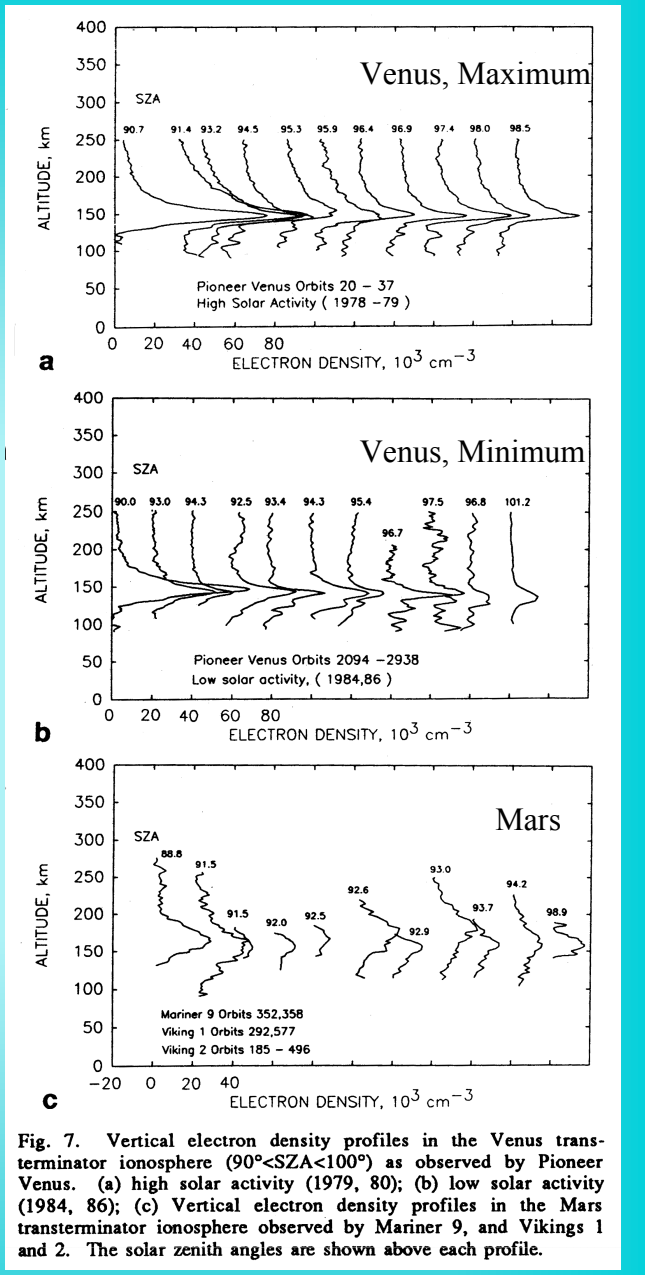

Fig. 7. Vertical electron density profiles in the Venus transterminator ionosphere (90°<SZA<100°) as observed by Pioneer Venus. (a) high solar activity (1979, 80); (b) low solar activity (1984, 86); (c) Vertical electron density profiles in the Mars transterminator ionosphere observed by Mariner 9, and Vikings 1 and 2. The solar zenith angles are shown above each profile.

電波掩蔽観測による電子密度プロファイル
Terminator付近。火星はピーク高度が広がっている。[Kliore, 1992]

Nightside Ionization Source

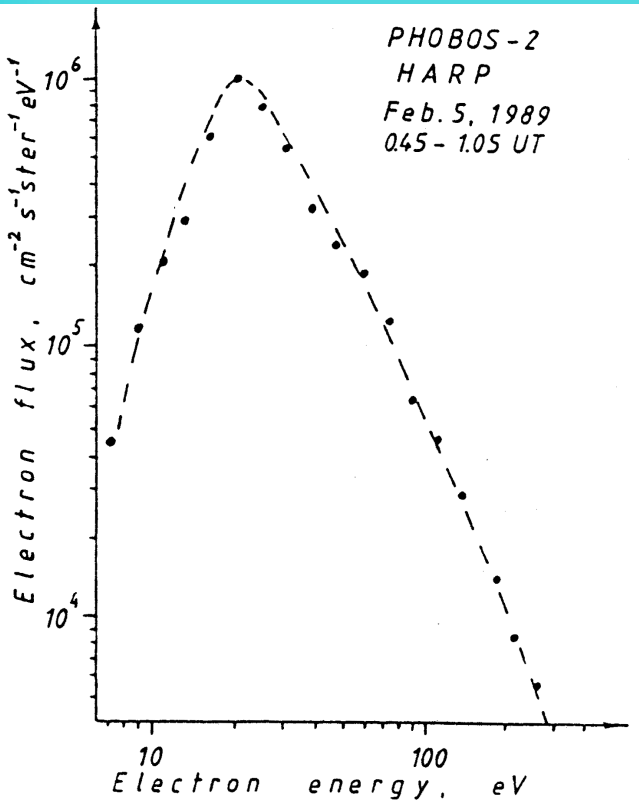

Fig. 3. The spectrum of electron fluxes averaged over a 20-min interval, characteristic of the Martian magnetotail lobes. The omnidirectional flux of electrons with energy E > 30 eV is approximately j ~ 2 x 10^8 cm^{-2} s^{-1}.

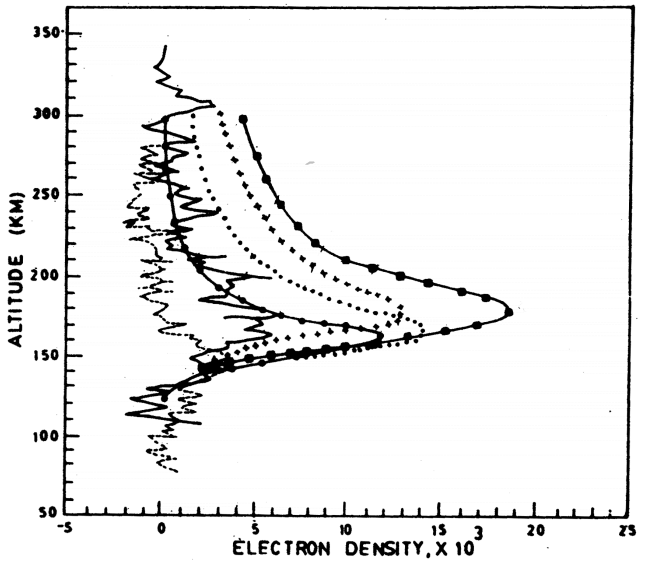

Figure 1. Electron density profiles in the nighttime ionosphere of Mars; dashed and solid lines show Viking 1 and 2 radio occultation measurements for orbits 374 and 216, respectively. line with solid circles, present calculation using analytical yield spectrum method and the source of magnetotail electron spectra; dotted line, multistream method using the source of magnetotail electron spectra [from *Fox et al.*, 1993]; plusses, multi stream method using the source of horizontal plasma transport [from *Fox et al.*, 1993]; lines with solid boxes, multistream method using the combined sources of magnetotail electron precipitation and horizontal plasma transport [from *Fox et al.*, 1993].

Phobos-2 HARP による低エネルギー電子の観測

Lobe領域、数十eVの低エネルギー電子flux。

[Verigin et al., 1991]

火星夜側電離圏電子密度プロファイルのモデル計算

電離源として電子降込、昼側からのプラズマ輸送を想定している。

[Haider, 1997]

References

Brace, L. H., R. F. Theis, H. G. Mayr, S. A. Curtis, and J. G. Luhmann, Holes in the nightside ionosphere of Venus, *J. Geophys. Res.*, 87, 199, 1982.

Fox, J. L., and A. J. Kliore, Ionosphere: Solar cycle variations, *Venus2*, 161-188,1997.

Haider, S. A., Chemistry of the nightside ionosphere of Mars, *J. Geophys. Res.*, 102, 407-416, 1997.

Kliore, A. J., Radio occultation observations of the ionosphere of Mars and Venus, *Venus and Mars: Atmosphere, Ionosphere, and Solar Wind Interactions, Geophysical Monograph 66,* AGU, 265-276, 1992.

Knudsen, W. C., P. M. Banks, and K. L. Miller, A new concept of plasma motion and planetary magnetic field for Venus, *Geophys. Res. Lett.*, 9, 7, 765-768, 1982a.

Knudsen, W. C., K. L. Miller, and K. Spenner, Improved Venus ionopause altitude calculation and comparison with measurement, *J. Geophys. Res.*, 87, 2246, 1982b.

Knudsen, W. C., The Venus ionosphere from in situ measurements, *Venus and Mars: Atmosphere, Ionosphere, and Solar Wind Interactions, Geophysical Monograph 66,* AGU, 237-263, 1992.

Knudsen, W. C. and K. L. Miller, Pioneer Venus suprathermal electron flux measurements in the Venus umbra, *J. Geophys. Res.*, 90, 2695-2702, 1985.

Luhmann, J. G., C. T. Russell, L. H. Brace, H. A. Taylor, W. C. Knudsen, F. L. Scarf, D. S. Colburn, and A. Barnes, Pioneer Venus observations of plasma and field structure in the near wake of Venus, J. Geophys. Res., 87, 9205-9210, 1982.

Marubashi, K., J. M. Grebowsky, H. A. Taylor, Jr., J. G. Luhmann, C. T. Russel, and A. Barnes, Magnetic field in the wake of Venus and the formation of ionospheric holes, *J. Geophys. Res., 90,* 1385-1398, 1985.

Miller, K. L., W. C. Knudsen, K. Spenner, R. C. Whitten, and V. Novak, Solar zenith angle dependence of ionospheric ion and electron temperature and density on Venus, *J. Geophys. Res.*, 85, 7759, 1980.

Taylor, H. A., Jr., H. C. Briton, S. J. Bauer, and R. E. Hartle, Global observations of the composition and dynamics of the ionosphere of Venus, implications for the solar wind interaction, *J. Geophys. Res.,* 85, 7765, 1980.

Theis, R. F., L. H. Brace, R. C. Elphic, and H. G. Mayr,New empirical models of the electron temperature and density in the Venus ionosphere with application to transterminator flow, *J. Geophys. Res.,* 89, 1477, 1984.

Verigin, M. I., K. I. Gringauz, N. M. Shutte, S. A. Haider, K. Szego, P. Kiraly, A. F. Nagy, and T. I. Gombosi, On the possible source of the ionization in the nighttime Martian ionosphere 1. Phobos 2 HARP electron spectrometer measurements, *J. Geophys. Res.*, 96, 19307-19313, 1991.